Photoacoustics 26 (2022) 100365

Contents lists available at ScienceDirect

Photoacoustics

journal homepage: www.elsevier.com/locate/pacs

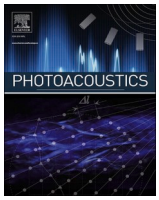

Photoacoustic graphic equalization and application in characterization of red blood cell aggregates

Lokesh Basavarajappa, Kenneth Hoyt *

Department of Bioengineering, University of Texas at Dallas, Richardson, TX, USA

ARTICLE INFO

Keywords:
Frequency analysis
Optical absorbers
Photoacoustics
Radiofrequency analysis
Tissue characterization
Ultrasound

ABSTRACT

A photoacoustic (PA) graphic equalization (PAGE) algorithm was developed to characterize the relative size of optical absorbing aggregates. This technique divides the PA signal into frequency bands related to different-sized optical absorbers. Simulations of a material containing optical absorbing microparticles of varying size were used to assess PAGE performance. Experiments were performed on phantom materials containing microspheres of varying size and concentration. Additional experiments were performed using tubes with fresh clotting blood. PA data was obtained using a Vevo LAZR-X system (FUJIFILM VisualSonics Inc). PAGE imaging of phantoms with varying-sized optical absorbers found a 1.5-fold difference in mean image intensity ($p < 0.001$). Conversely, PA images from these same materials exhibited no intensity changes ($p = 0.68$). PAGE imaging results from clotting blood exhibited differences for clot sizes in the range 0.30–0.64 mm ($p < 0.001$). In summary, PAGE imaging can distinguish optical absorbing aggregates of varying size.

1. Introduction

Photoacoustic (PA) imaging combines both optical and ultrasound modalities to obtain images detailing optical absorption [1]. In practice, the target tissue or material to be imaged is optically excited, which leads to a transient temperature rise, thermoelastic expansion of the optical absorbers, and then emission of ultrasound pressure waves. The emitted pressure waves are detected using standard ultrasound transducers and images are generated using reconstruction algorithm to represent a spatial map of tissue absorption. The main endogenous optical absorbers in tissue include lipids, water, and chromophores like hemoglobin and melanin, versus exogenously delivered contrast agents. Given the unique optical absorption properties of deoxygenated and oxygenated hemoglobin in the near infrared wavelength range, hemoglobin is a popular target of PA imaging to visualize blood vessels [2]. PA imaging has achieved considerable progress in both the preclinical and clinical settings because it provides both high contrast and high spatial resolution in tissues [3,4].

PA images are reconstructed using the envelope of recorded PA signals from underlying tissue. This procedure is very similar to brightness-modulated (B-mode) ultrasound imaging, except intensity in PA imaging is governed by optical absorption in comparison to ultrasound images that are based on local variations in acoustic impedance [5]. However, a nonlinear relationship between the time-dependent PA signal and optical absorption leads to inaccurate tissue characterization when using PA images [6]. Therefore, considerable research has focused on finding encoded features in the local PA data that could reveal additional information about tissue function and pathology that cannot be seen in the more conventional PA images. To that end, spectral parameters like spectral slope, mid-band fit, and y-intercept, can be extracted from the calibrated power spectrum of the time-dependent PA signal and used for quantitative tissue characterization. This frequency-domain analysis is adapted from ultrasound imaging methods used for tissue characterization [7]. Therefore, it is reasonable to assume that spectral parameters from the PA signal will allow similar interpretations as those extracted from ultrasound data.

Several *in vivo* preclinical studies using cancer-bearing animals have demonstrated that spectral parameter estimations from normal tissue and malignant tumors were significantly different [8,9]. More specifically, a frequency analysis of PA signals from capillaries revealed a quantitative relationship between blood vessel diameter and spectral slope [10]. Given PA spectral parameters are related to the chromophore microstructure, they can be used to estimate the size and shape of the optical absorbers [11]. PA signal-derived spectral parameters were then shown helpful for the detection of tumor changes after administration of a vascular-disrupting agent [12,13]. In simulations, Rayleigh and

* Corresponding author.
E-mail address: kenneth.hoyt@utdallas.edu (K. Hoyt).

https://doi.org/10.1016/j.pacs.2022.100365
Received 14 February 2022; Received in revised form 15 April 2022; Accepted 6 May 2022
Available online 9 May 2022

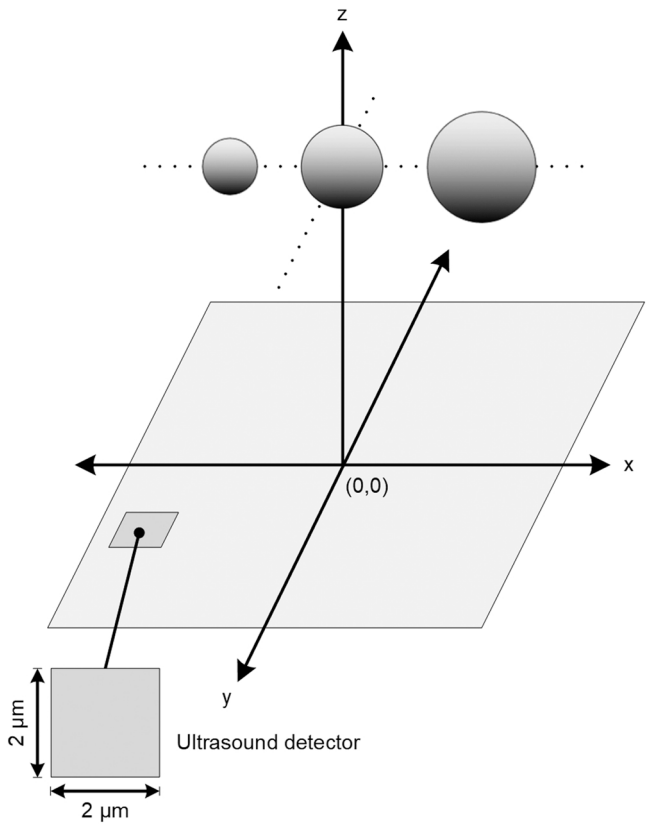

Fig. 1. Description of the numerical phantom with spatial measurement geometry in the *x*, *y*, and *z* planes relative to the origin. Three different-sized optical absorbers with diameters of 10, 40, and 100 μm, were evenly distributed at a depth of $z = 40$ μm. A rectangular ultrasound detector of size 2×2 μm was created and moved using a spatial sampling period of 2 μm to scan the *xy* plane at fixed depth.

Nakagami distribution parameters from the power spectrum were found to differentiate normal and intratumoral vascular structures [14]. In another study, size and concentration of regularly-shaped PA absorbers were estimated quantitatively using a wavelet-domain analysis of PA signals [15]. Frequency-modulated (F-mode) imaging is another quantitative PA technique that was introduced to allow visualization of optical absorbing structures of different scale [16]. This method uses selective spectral bands to detect small deviations in object size (or shape) and produce PA images with scale-specific contrast. In approach, these scale-specific images were generated by appropriately dividing the power spectrum of the PA signals and then utilizing spectral features from the subdivisions. It has been shown that F-mode PA imaging can be used for a range of purposes including visualization of organelles in cultured cells for selective display to single blood vessels in zebrafish larvae.

In the ultrasound research community, H-scan (where the 'H' stands

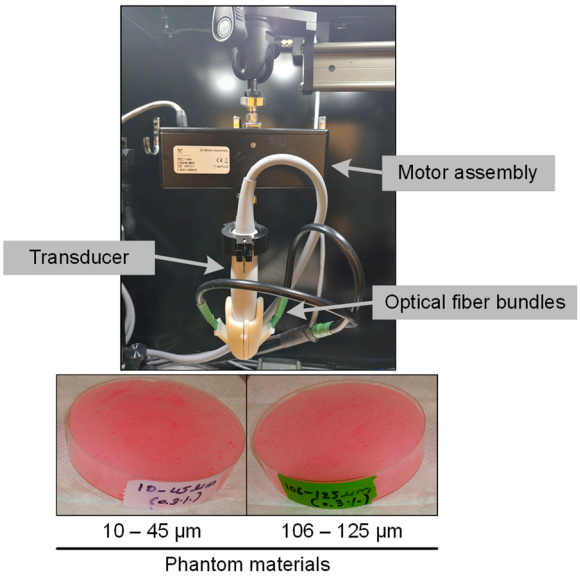

Fig. 3. Experimental setup detailing the ultrasound transducer, optical fiber bundle, and motor assembly for acquiring data in space. Also shown are digital images of representative phantom materials containing optical-absorbing microspheres of different diameter (10–45 or 106–125 μm).

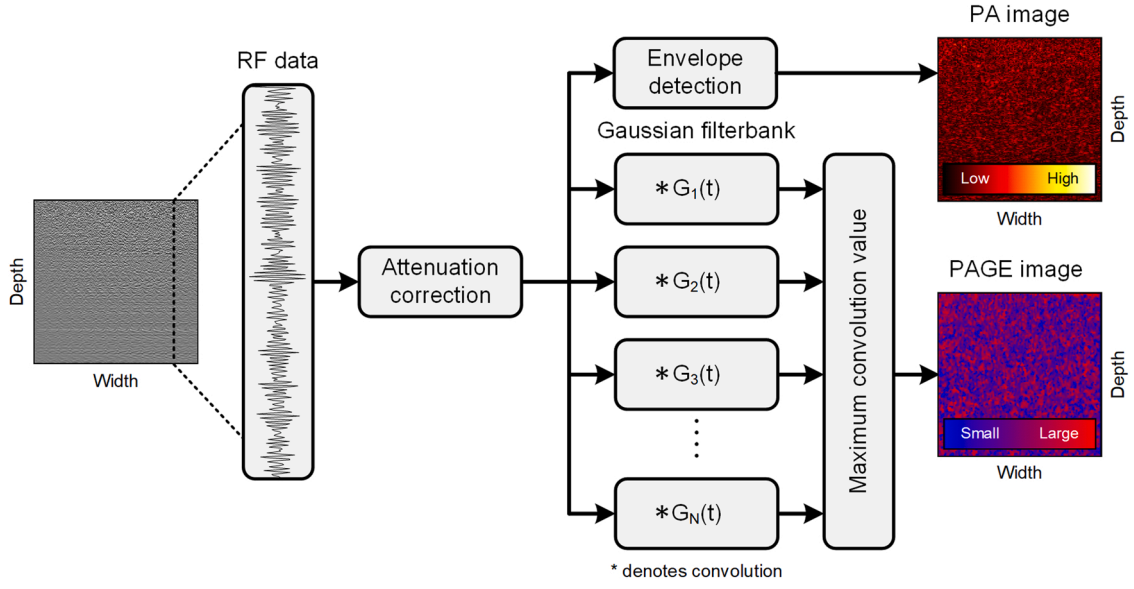

Fig. 2. Schematic diagram detailing the sequence of photoacoustic (PA) signal processing steps for reconstruction of the PA graphic equalization (PAGE) image. Given PA data in radiofrequency (RF) format, ultrasound attenuation correction is applied before application of a Gaussian bandpass filter bank. Time-domain signal processing uses an ensemble of convolutional filter and the maximum convolution value at each pixel location is used to generate the PAGE image intensity.

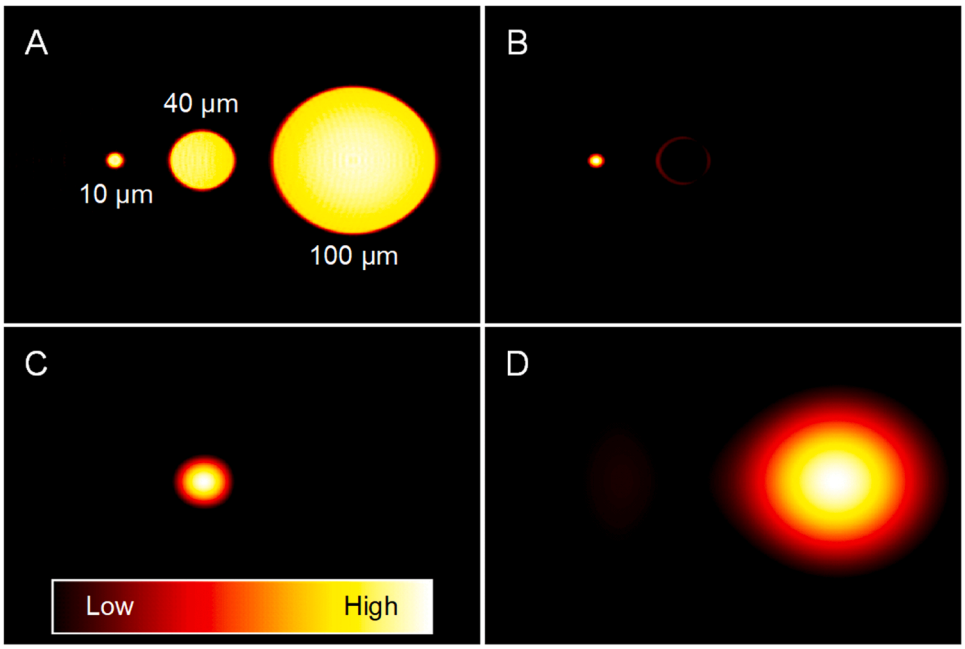

Fig. 4. Images are from numerical simulation, (A) reconstructed PA image without filtering, and PA data processed with different matched filters with a center frequency (60% bandwidth) of (B) 150 (90) MHz, (C) 60 (36) MHz, or (D) 15 (9) MHz before PAGE image reconstruction.

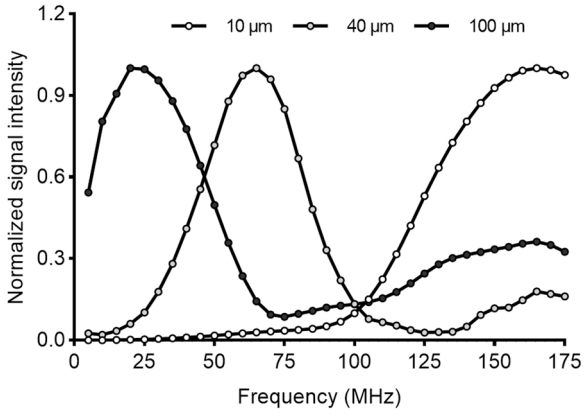

Fig. 5. Normalized signal intensity profile plots from different sized optical absorbers and simulated PAGE images processed using different bandpass filter center frequencies ranging from 5 to 175 MHz with frequency sampling period of 5 MHz.

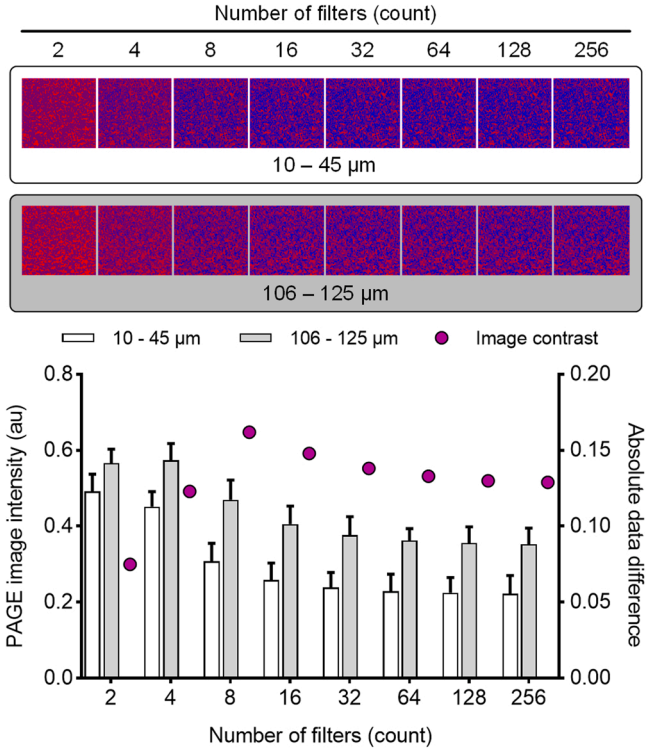

Fig. 6. PAGE images and their intensity plot from phantom materials embedded with varying sized optical absorbers (0.3% concentration) following image reconstruction using different filter counts. Absolute data difference (image contrast) was calculated from PAGE image intensities of phantom materials containing different sized optical-absorbing microspheres.

for Hermite or hue) imaging has been introduced for high-resolution tissue characterization [17]. It is founded on the assumption that smaller scatterers produce higher frequency content in the back-scattered ultrasound signals whereas larger scatterers generate the lower frequency signal components. Unique frequency information is extracted using a set of matched filters corresponding to specific sized ultrasound scatterers. Output from the matched filters is then weighted and used to colorize an image to provide local discrimination between various-sized ultrasound scatterers. Several recent reports have detailed the use of *in vivo* H-scan ultrasound imaging for purposes ranging from the early detection of liver steatosis [18–20] to monitoring cancer response to treatment [21–23]. We envision that the H-scan ultrasound format for tissue characterization can be extrapolated for a similar analysis of PA signals.

In stereophonic sound systems, graphic equalization is a popular output control strategy that divides the audio signal into many different frequency bands that are centered at a specific frequency and gain adjusted to listener preference. Adapted from this technique and theoretical considerations, the research presented here details the use of a novel PA graphic equalization (PAGE) algorithm to depict the relative size of optical absorber aggregates. This PAGE algorithm is a modified H-scan ultrasound data processing approach for the analysis of PA signals. In short, it divides the recorded PA signal into a collection of

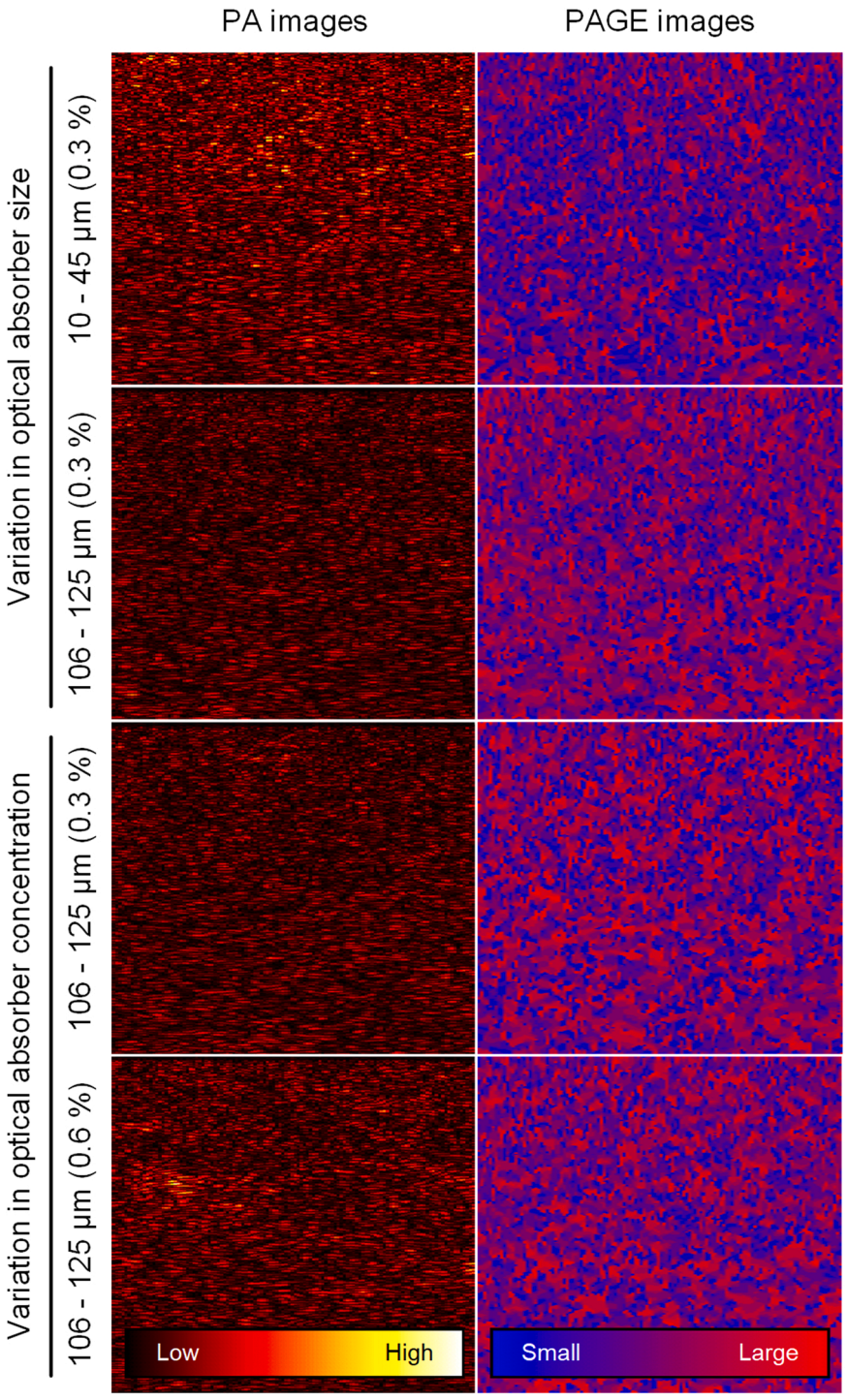

Fig. 7. Co-registered PA images (left) and PAGE images reconstructed with filter count 8 (right) obtained from phantom materials containing different sized spherical optical-absorbing microspheres (10–45 μm and 106–125 μm) and different concentrations (0.3% and 0.6%). The PAGE image colormap denotes relatively small to large optical absorber size and ranges from blue to red, respectively.

frequency bands using a filterbank, and outputs are used to colorize a display to allow tissue characterization functionality. In this paper, we expand the PAGE format and introduce a new signal processing and image reconstruction approach. Theoretical formulations are introduced and experimental validation was performed using a series of *in vitro* phantom material and *ex vivo* whole blood clot studies.

2. Methods

2.1. Theoretical formulation of the PAGE algorithm

In response to a heat source, the pressure $p(r,t)$ at position r and time t in an isotropic, acoustically homogeneous, and inviscid fluid medium obeys the following equation [24]:

$$\left(\nabla^2 - \frac{1}{c^2}\frac{\partial^2}{\partial t^2}\right)p(r,t) = -\frac{\beta}{c_p}\frac{\partial}{\partial t}H(r,t) \quad (1)$$

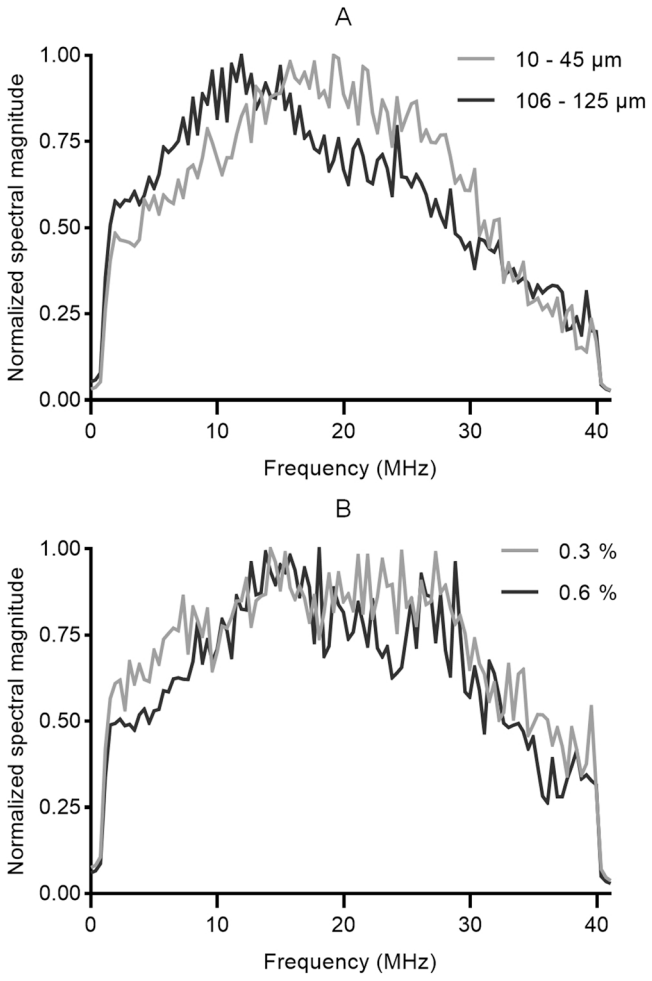

Fig. 8. Frequency spectra from phantom materials embedded with (A) different sized optical absorbers (fixed concentration of 0.3%) and (B) different concentrations of optical absorbers (fixed size of 106–125 μm). Note the change in peak frequency observed only in different sized optical absorbers.

where c is the speed of sound, β is the isobaric volume expansion coefficient, c_p is the specific heat, and $H(r,t)$ is the heating function defined as the thermal energy deposited by the energy source as a function of time and space. The spatiotemporal heating function can be further written as:

$$H(r,t) = A(r)I(t) \tag{2}$$

where $A(r)$ is the spatial absorption function and $I(t)$ is the temporal illumination function of the optical source. The latter can be considered a short pulse like a Dirac delta function:

$$I(t) = \delta(t) \tag{3}$$

Substituting Eqs. (2) and (3) into Eq. (1) and then taking the Fourier transform on variable $\bar{t} = ct$ yields the following:

$$\left(\nabla^2 + k^2\right)P(r,k) = jkc^2\frac{\beta}{c_p}A(r) \tag{4}$$

where $P(r,k)$ is the frequency spectrum of the thermoacoustic signal $p(r,t)$ and k the ultrasound wave number. Note that Eq. (4) represents an inhomogeneous Helmholtz wave equation. Assuming that $p(r,t)$ is measured on a surface S_0 that encloses some sample of interest, the spectrum $P(r_0,k)$ of the pressure $p(r_0,\bar{t})$ detected at the position r_0 can be written as follows [24,25]:

$$P(r_0,k) = -jk\iiint_V d^3r\widetilde{G}_k(r,r_0)p_i(r) \tag{5}$$

where $p_i(r)$ is initial photoacoustic pressure, $p_i(r) = A(r)c^2\beta/c_p$ and $\widetilde{G}_k(r,r_0)$ is a Green's function described as:

$$\widetilde{G}_k(r,r_0) = \frac{1}{4\pi|r-r_0|}e^{jk|r-r_0|} \tag{6}$$

In principle, a Dirichlet Green's function $\widetilde{G}_k^D(r,r_1)$ can be constructed that satisfies the boundary condition $\widetilde{G}_k^D(r,r_1) = 0$ for r_1 on S and r inside S. According to Green's theorem, the ultrasound pressure $P(r,k)$ inside the surface S can be computed by the surface integral:

$$P(r,k) = \int_S \mathrm{d}SP(r_0,k)\left[n_0^s\nabla_0\widetilde{\mathrm{G}}_{\mathrm{k}}^{(\mathrm{D})}(r,r_0)\right] \tag{7}$$

where ∇_0 denotes the gradient over a variable r_0 and n_0^s is the normal of surface S pointing to the source. For planar geometry, the Green's function can be simplified and the reconstruction formula can be written as a universal backprojection formula [26,27]:

$$P_0^{(b)}(r) = \frac{1}{\pi}\int_S \mathrm{d}S\int_{-\infty}^{\infty}\mathrm{d}kP(r_0,k)\left[n_0^s\nabla_0\widetilde{G}_k^{(in)}(r,r_0)\right] \tag{8}$$

where $P_0^{(b)}(r) = P_0^{(b)}(r,\bar{t}=0)$. The ultrasound pressure field $P(r_0,k)$ can be simulated using a defined measurement geometry [6]. Photoacoustic signals from uniform spherical absorbers after Dirac delta function (δ) illumination is then calculated by:

$$P(r_0,k) = \mathscr{F}[A_0U(a-|R-ct|)(R-ct)/2R] \tag{9}$$

where $\mathscr{F}$ denotes Fourier transform function, A_0 is the intensity, a is the radius of spherical absorbers, and R is the distance between the detector position and absorber center. The operator U is a step function and it is defined as:

$$U(l) = \left\{\begin{array}{l} 1, \text{ when } l > 0 \\ 0, \text{ when } l \le 0 \end{array}\right\} \tag{10}$$

Frequency content of the pressure field will be distinct when optical absorbers of different size are present. Therefore, the ultrasound pressure field can be multiplied by a properly constructed bandpass filter to isolate information related to different-sized optical absorbers. An arbitrary bandpass filter of Gaussian type is described by the following formula:

$$\widetilde{W}_c(k) = e^{-\left[\left(k^2-k_0^2\right)/kW\right]^2} \tag{11}$$

where $k_0 = 2\pi f_0/c$, f_0 is the center frequency and W is the width of the filter passband. Calculating the inverse Fourier transform of Eq. (8) yields the following time-domain expression [27]:

$$p_0^{(b)}(r) = -\frac{2}{\Omega_0}\nabla\int_{S_0} n_0^s dS_0\left[\frac{p(r_0,\bar{t})}{\bar{t}}\right]_{\bar{t}=|r-r_0|} \tag{12}$$

Further, Eq. (12) can be rewritten in a clear backprojection form as follows:

$$p_0^{(b)}(r) = \int_{\Omega_0} b(r_0,\bar{t}=|r-r_0|)d\Omega_0/\Omega_0 \tag{13}$$

where $b(r_0,\bar{t}) = 2p(r_0,\bar{t}) - 2\bar{t}\partial p(r_0,\bar{t})/\partial\bar{t}$ is the backprojection term related to measurements at position r_0 and $d\Omega_0 = \frac{dS_0}{|r-r_0|^2}\bullet[n_0^s.(r-r_0)/|r-r_0|]$ is the solid angle for a detection element dS_0 with respect to a reconstruction point.

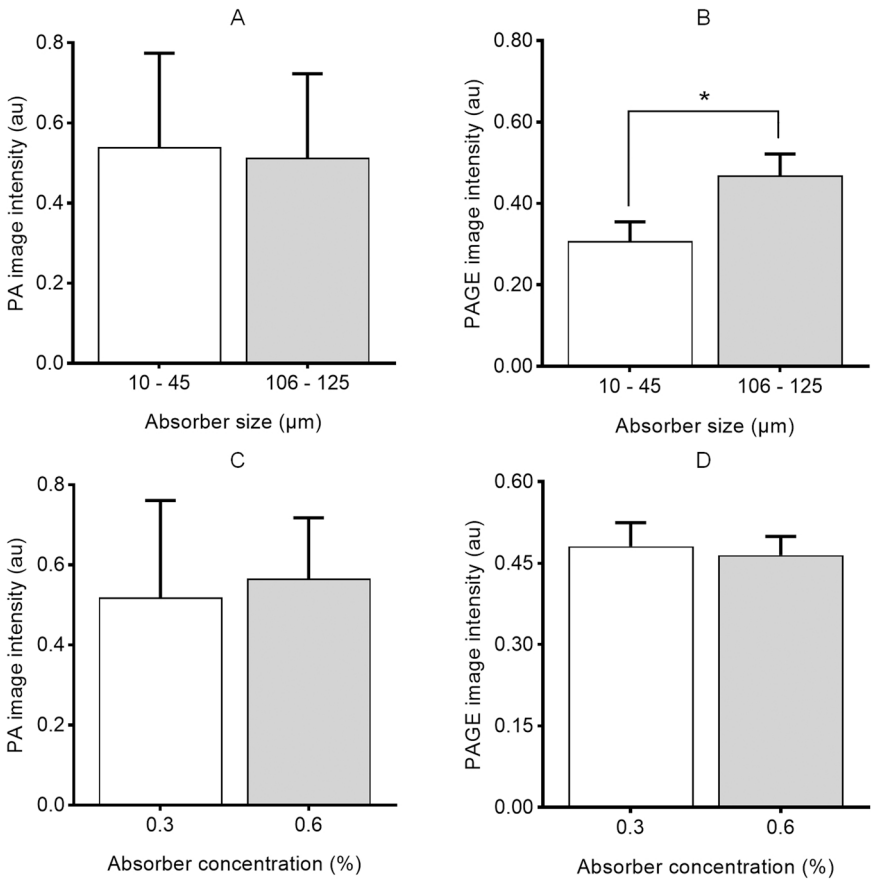

Fig. 9. Summary of mean PA and PAGE image intensities from phantom materials embedded with different (A, B) concentrations of optical absorbers or (C, D) sized optical absorbers. A * denotes a p-value < 0.05.

2.2. Theory implementation

Theoretical formulations were implemented in MATLAB R2020 (MathWorks, Inc., Natick, MA) to produce spatial (2-dimensional, 2-D) images. A numerical phantom was created as shown in Fig. 1. Three different-sized optical absorbers with diameters of 10, 40, and 100 μm were positioned at spatial coordinates (−80, 0, 40), (−25, 0, 40), and (70, 0, 40) μm, respectively. Volume data was obtained by scanning the entire geometry. For illustration, we scan the xy plane by defining a rectangular shaped ultrasound detector of size 2×2 μm with a spatial sampling period of 2 μm at a depth of $z = 40$ μm. A finite detector of size 2×2 μm was used in the study, which allowed simulation of optical absorber sizes as small as 4 μm. The center of the detector surface represents the detector position. The entire xy plane is divided into a 151×151 grid to cover x and y axes of range -150 to 150 μm. For ease of computation, the detector surface was subdivided into 25 smaller elements. The total ultrasound pressure signal at the detector was then computed to obtain $P(r_0, k)$ using Eq. (9). Then an ensemble of Gaussian bandpass filters as described by Eq. (11) with different center frequencies (60% bandwidth) were utilized to isolate specific frequency content. Finally, the inverse Fourier transform of the product $\widetilde{W}_c(k) \bullet P(r_0, k)$ was calculated and used in Eq. (13) to compute the reconstructed PA image.

2.3. PA data acquisition

Imaging was performed using a preclinical PA scanner (Vevo LAZR-X, FUJIFILM VisualSonics Inc, Toronto, Canada) equipped with a 21 MHz center frequency linear array transducer (MX250D) with an effective bandwidth from 15 to 30 MHz. A pulsed optical parametric oscillator (OPO) laser was pumped by a doubled Nd:YAG source with pulse width and energy of 5 ns and 45 mJ, respectively. The laser was tuned to a wavelength of 680 nm and delivered by optical fiber bundles mounted on each side of the ultrasound transducer used for data acquisition of an illuminated sample. In-phase and quadrature (IQ) data was collected from different image planes by precise movement of the fixed transducer using a 3-dimensional (3-D) motorized system (Vevo Imaging Station, FUJIFILM VisualSonics Inc) along the elevational direction (total of 30 frames equally spaced 3 μm apart). Saved IQ data was then upsampled to radiofrequency (RF) format prior to PA and PAGE image reconstruction.

2.4. PAGE Image reconstruction

All recorded PA data was corrected for one-way ultrasound signal attenuation using global scaling and assuming a nominal value of 0.5 dB/cm/MHz. Attenuation compensated PA signals were convolved with a matched Gaussian filterbank that were equally spaced to span the entire transducer bandwidth (N distinct peak frequencies). This application of parallel filtering yielded distinct convolutional values between the different Gaussian functions and PA data. At each pixel, the filter output yielding the maximum convolutional value was selected. Lower and higher frequency values were then assigned to a red (R) and blue (B) channel, respectively, yielding a colormap scheme with dynamic range of N levels. The final PAGE image intensity was calculated as a ratio of the R channel to the sum of the R and B channel data. To understand the influence on PAGE image reconstruction, we evaluated the use of different filter count 2^N for $N = 0, 1, \ldots, 8$, during the matched filtering process. The -6 dB bandwidth of these bandpass filters was set to 7.5 MHz. A generalized schematic of the PAGE image reconstruction

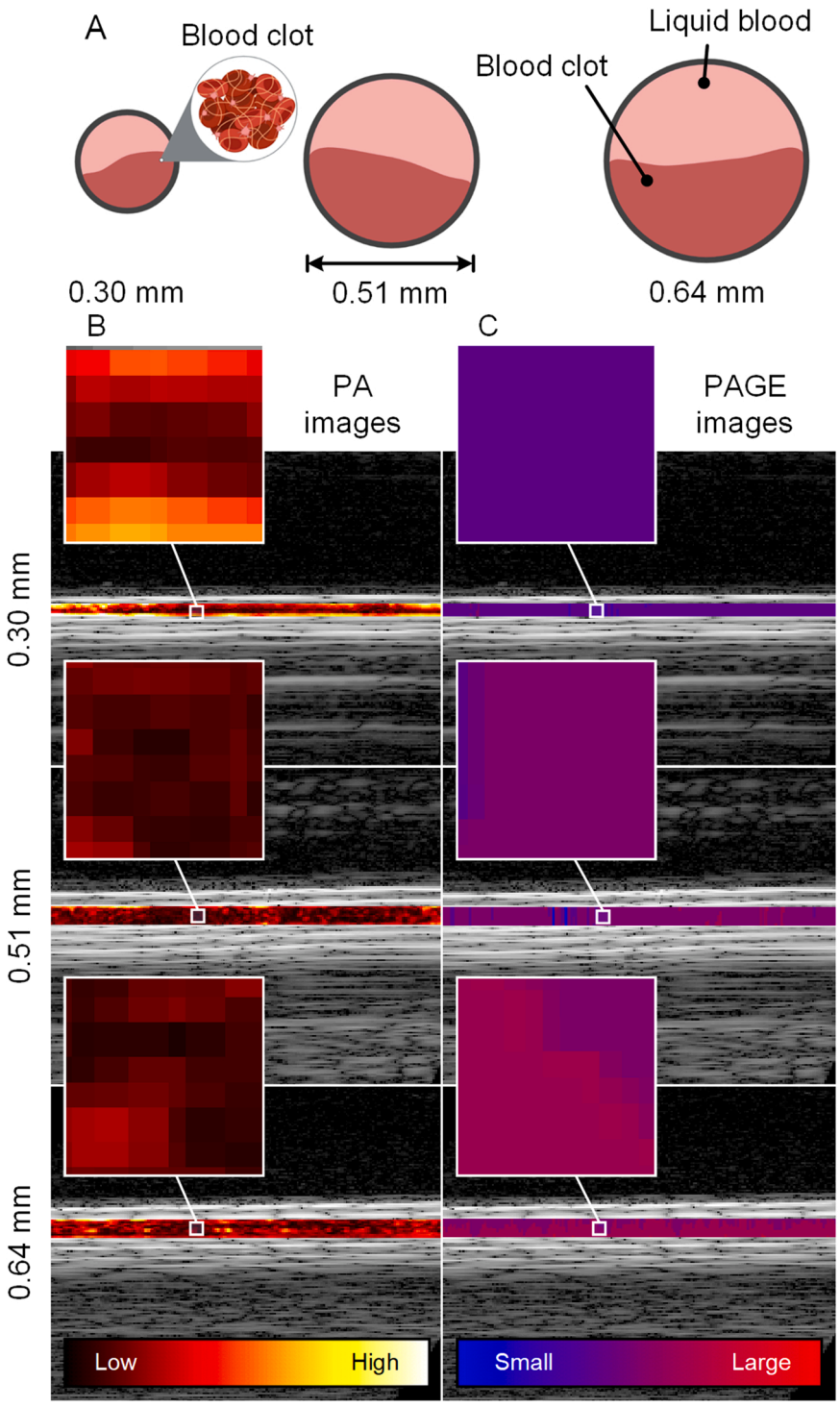

Fig. 10. (A) Schematic illustration of formation of blood clot in translucent tubes. (B) PA and (C) PAGE images of blood clots formed in tubes with a lumen diameter of 0.30, 0.51, or 0.64 mm. Note the progressive changes in PAGE image intensity as vessel diameter and the blood clot size was increased.

procedure is illustrated in Fig. 2. Traditional PA images were produced by computing the envelope of the attenuation corrected RF data via a Hilbert transformation and displayed the final image. The dynamic range of all images was set to 8-bit format.

2.5. Experimental setup

Homogeneous phantom materials were prepared by introducing agar and various-sized optical absorbers (fluorescent polyethylene microspheres, CoSpheric LLC, Santa Barbara, CA) to 0.3 L of degassed water [28]. The solution was slowly stirred and heated to 65 °C before transferring to a rigid mold (radius × height = 4.3 × 1.8 cm). Phantoms were stored at 4 °C and allowed to cool overnight before use. A total of four different phantoms were created to study the impact of optical absorber size (diameters of 10–45 or 106–125 μm) and concentration (0.3 or 0.6%) on *in vitro* PA and PAGE imaging. Next, translucent silicone elastomer tubes (Liveo, Thermo Fisher Scientific, Waltham, MA) with inner lumen diameters of 0.30, 0.51, or 0.64 mm were used for an *ex vivo* study. Picture of phantom materials along with an experimental setup is shown in Fig. 3. Tubes were carefully filled with freshly drawn blood

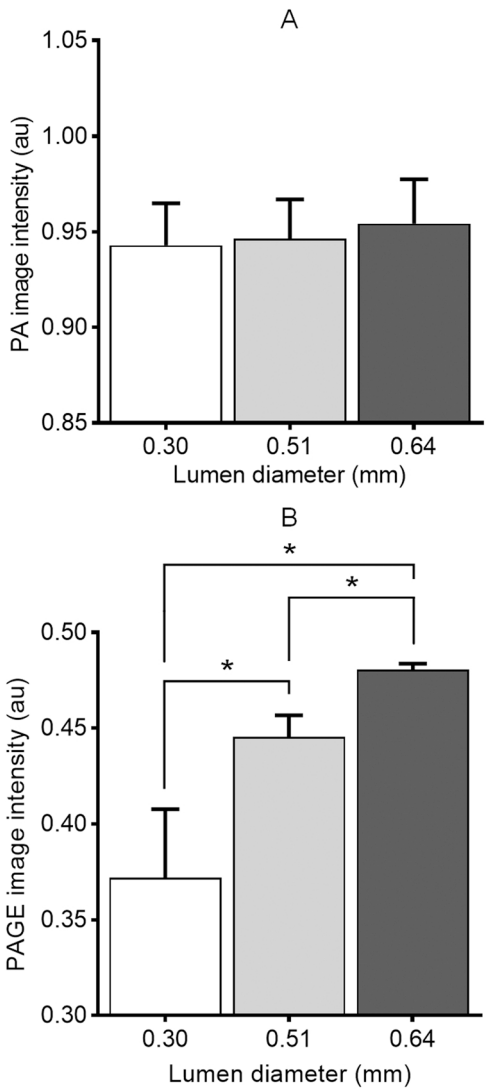

Fig. 11. Summary of mean PA (top) and PAGE (bottom) image intensity results from translucent tubes containing blood clots that were either 0.30, 0.51, or 0.64 mm in size. A * denotes a p-value < 0.05.

from healthy rats scheduled for euthanasia and allowed to clot for 1 h. Note that blood clots were formed after being separated from liquid blood and size of each clot was less than the lumen diameter. PA and PAGE imaging of each blood sample was then performed by positioning the ultrasound transducer lengthwise along the tubes after submerging the area of interest at depth in a water bath.

2.6. Statistical analysis

Both PA and PAGE images were used for statistical analysis and intensity was summarized as the mean ± standard deviation (SD). Relationships between different samples was assessed using a Mann-Whitney U test. A p-value less than 0.05 was considered statistically significant. Analyses were performed using Prism 9.2 (GraphPad Software Inc, San Diego, CA).

3. Results

Numerical simulations were performed by implementing theoretical formulations for a specified measurement geometry as described in Fig. 1. Traditional PA and PAGE images were reconstructed from an *in silico* material containing three spaced spherical optical absorbers of differing size. A series of reconstructed PA images without frequency filtering and also after PAGE processing with matched bandpass filter use are shown in Fig. 4. Simulated PAGE images were filtered at center frequencies of 150, 60, and 15 MHz to help localize the 10, 40, and 100 μm-sized optical absorbers, respectively. This example highlights the relationship between optical absorber size and production of local frequency content in the PA signal. A summary of optical absorber localizations at different center frequencies ranging from 5 to 175 MHz with a sampling of 5 MHz is plotted in Fig. 5. Signal intensity from different size optical absorbers was calculated using corresponding absorber sized region of interest. It is noted that the signal intensity measurements from the smaller absorber (10 μm) region have a peak value at a higher center frequency and that from the larger absorber (100 μm) peaks at a much lower frequency, which is consistent with theoretical predictions.

Homogeneous phantom materials were prepared to contain optical absorbers of varying size (i.e., 10–45 or 106–145 μm) and concentration (i.e., 0.3 or 0.6%). To assess the impact of filter count on PAGE image intensity, a series of image reconstructions were performed using matched filter banks with 2 to 256 equally spaced bandpass filters. Reconstructed PAGE images and corresponding intensity plots are presented in Fig. 6. It can be observed that PAGE image intensity decreases as the filter count increases and remains relatively constant after a filter count of 32. This is due to the increased filter count and corresponding changes in filter overlap (spectral correlation). Assuming absolute differences between data acquired in phantoms embedded with the two dissimilar sized optical absorbers is a surrogate measure of PAGE image contrast, this contrast is maximized using a filter count of 8 and then gradually decreases from a maximum of 0.16 to 0.13 as the number of filters used during reconstruction is increased from 8 to 256. Hereafter, all PAGE images were reconstructed using 8 equally spaced Gaussian bandpass filters that encompassed the entire US transducer bandwidth (i.e., 15–30 MHz).

Co-registered PA and PAGE images of homogeneous phantom materials prepared using various sized optical absorbers (i.e., 10–45 or 106–145 μm) and concentrations (i.e., 0.3 or 0.6%) are presented in Fig. 7. While the PA images obtained from these phantom materials did not exhibit any qualitative differences, PAGE images from the phantom embedded with the larger optical absorbers displayed a notable redder hue. Specifically, mean PAGE image intensity from the phantoms with the smaller and larger optical absorbers were 0.30 ± 0.04 and 0.47 ± 0.05, respectively. Conversely, there was no observed change in either the PA or PAGE images when the concentration of the optical absorbers was varied. Normalized spectral plots of the corresponding PA data are shown in Fig. 8. Inspection of these plots reveal a change in the peak frequency for data from phantoms embedded with different sized optical absorbers. Conversely, no change was found in the PA data from phantoms embedded with different concentrations of the same sized optical absorbers. A summary of all *in vitro* PA and PAGE imaging results are plotted in Fig. 9. These quantitative measures reveal statistically significant difference in mean PAGE image intensity was found when imaging the phantom materials embedded with the two different sized optical absorbers ($p < 0.001$). No differences were found in the co-registered PA images ($p = 0.68$). For phantom materials containing different concentrations of equal sized optical absorbers, no differences were found in either the mean PAGE ($p = 0.29$) or PA ($p = 0.76$) image intensities.

Fresh blood was transferred to translucent tubes with different lumen size and imaged after allowing clots to form for 1 h. Co-registered PA and PAGE images were reconstructed and overlaid on conventional grayscale ultrasound images for visual guidance, Fig. 10. Notice the image panel indicates a progressive hue shift from bluer to redder as the size of the blood clots increased. A summary of PA and PAGE image intensities are plotted in Fig. 11. These results reveal statistically significant differences between the PAGE images of blood clots in the size range from 0.30 to 0.64 mm ($p < 0.001$). Contrarywise, no significant

differences were found in the analysis of the co-registered PA images ($p > 0.08$).

4. Discussion

This study introduced the PAGE algorithm for the analysis of recorded PA signals to reveal encoded information about the local size of optical absorbing aggregates. Numerical simulations were implemented and experiments were performed using phantom materials and translucent tubes containing blood clots to study the PAGE approach. Both simulated and experimental data processed using different matched bandpass filters revealed the PAGE format can accurately depict the relative size of different optical absorbers. No notable change was observed in the PAGE images when different concentrations of the same-sized optical absorbers were used. These results were then validated by PAGE imaging of formed blood clots of varying size.

The broadband nature of the PA signal is desirable for frequency analysis methods. However, presence of speckle makes it difficult to isolate scale specific structures of a particular frequency. In previous research, it was shown that PA speckle can develop from non-resolvable structures such as multiple absorbers and tissue microvascularity [29]. The appearance of speckle curtails the accuracy of frequency analysis methods that extract information from specified frequency bands like F-mode PA imaging. Quantitative methods, such as spectral slope and mid-band fit, are system independent approaches relying on the analysis of the recorded PA signals to quantify structural information in the presence of speckle. These methods require reference phantom measurements (tissue equivalent calibration standard) that are used to remove the impact of imaging system settings during data acquisition. In comparison, the proposed PAGE algorithm does not require reference measurements. Limitations of the PAGE algorithm are it yields relative measures of optical absorber size and results are affected by attenuation compensation methods. In this study, we only considered and compensated for ultrasound attenuation, as that has been shown to produce clear improvements in the magnitude and resolution of the reconstructed PA images [30].

Results from the PAGE approach showed that PAGE images can differentiate optical absorbers of varying size. This is due to the bandpass filtering of PA signals using filters with limited bandwidth. Further, simulation results revealed that very small optical absorbers (i.e., less than 10 μm like a red blood cell) can be isolated with high frequencies above 100 MHz, but this is not realistic prospect given basic ultrasound physics considerations and current linear array transducer technology. From phantom materials results, it was noted that the PAGE image intensity changed with the filter count used during image reconstruction. Interestingly, filter count corresponds to the degree of spectral overlap between neighboring filters. For example, a filter count of 4 corresponds to a 50% overlap, 8–75%, 16–90%, 32–95%, and so on. Due to a high degree of spectral correlation using a higher number of filters, we did not observe any major change in the PAGE images that were processed using a matched filter count above 32. The spectral overlap between filters can also be changed by varying filter width.

The PAGE algorithm can be used in clinical applications like for the detection of red blood cell aggregation, cancer treatment progression, identification of histological microfeatures, etc. Red blood cell aggregation is a particularly important biomarker for a variety of blood disorders and clinical conditions that include bacterial infections, diabetes, myocardial infarction, and sickle cell disease. Noteworthy, it was previously shown that PA signal-derived spectral parameters from red blood cell aggregates could be used to differentiate the clusters due to varying hematocrit levels [31,32]. Compared to data acquired from a blood clot formed in a vessel with a 0.30 mm inner lumen diameter, mean PAGE image intensity measurements were found to increase by 21.6% and 29.7% when imaging the 0.51 and 0.64 mm vessels, respectively. Future work may explore the use of the PAGE approach for detecting physical changes in the tumor microvascular network (morphology) during both cancer growth and drug treatment [13,33]. A spectrogram of PA signals also reveals unique molecular and chemical components for specific tissue types along with corresponding histological microfeatures. This could contribute to the diagnosis and management of other diseases involving diffusive patterns such as found in fatty liver [34].

5. Conclusions

The PAGE format was introduced as a new modality for soft tissue characterization that divides the PA signal into an ensemble of different frequency bands used for image reconstruction. PAGE imaging was investigated using numerical simulations, homogeneous phantom materials embedded with optically absorbing microspheres, and various sized blood clots formed inside translucent tubes. Overall, it was shown that PAGE imaging can distinguish smaller optically absorbing objects of varying sizes. Analysis of the ensemble filter count during PAGE image reconstruction demonstrated that intensity corresponds to spectral overlap (correlation) of the filter banks used.

Declaration of Competing Interest

The authors declare the following financial interests/personal relationships which may be considered as potential competing interests: Kenneth Hoyt reports financial support was provided by the National Institutes of Health and Cancer Prevention and Research Institute of Texas.

Acknowledgments

This research was supported in part by National Institutes of Health (NIH) grants R01DK126833 and R01EB025841, and award RP180670 from the Cancer Prevention and Research Institute of Texas (CPRIT) to establish the Small Animal Imaging Facility at the University of Texas at Dallas. The authors would like to thank Junjie Li, PhD, for assisting with the blood clot experiments.

References

[1] P. Beard, Biomedical photoacoustic imaging, Interface Focus 1 (2011) 602–631.
[2] J. Yao, L.V. Wang, Sensitivity of photoacoustic microscopy, Photoacoustics 2 (2014) 87–101.
[3] S. Mallidi, G.P. Luke, S. Emelianov, Photoacoustic imaging in cancer detection, diagnosis, and treatment guidance, Trends Biotechnol. 29 (2011) 213–221.
[4] L.V. Wang, J. Yao, A practical guide to photoacoustic tomography in the life sciences, Nat. Methods 13 (2016) 627–638.
[5] M.N. Fadhel, E.S.L. Berndl, E.M. Strohm, M.C. Kolios, High-frequency acoustic impedance imaging of cancer cells, Ultrasound Med. Biol. 41 (2015) 2700–2713.
[6] S. Wang, C. Tao, Y. Yang, X. Wang, X. Liu, Theoretical and experimental study of spectral characteristics of the photoacoustic signal from stochastically distributed particles, IEEE Trans. Ultrason. Ferroelectr. Freq. Control. 62 (2015) 1245–1255.
[7] M.L. Oelze, J. Mamou, Review of quantitative ultrasound: Envelope statistics and backscatter coefficient imaging and contributions to diagnostic ultrasound, IEEE Trans. Ultrason. Ferroelectr. Freq. Control. 63 (2016) 336–351.
[8] R.E. Kumon, C.X. Deng, X. Wang, Frequency-domain analysis of photoacoustic imaging data from prostate adenocarcinoma tumors in a murine model, Ultrasound Med. Biol. 37 (2011) 834–839.
[9] S. Sinha, N.A. Rao, B.K. Chinni, V.S. Dogra, Evaluation of frequency domain analysis of a multiwavelength photoacoustic signal for differentiating malignant from benign and normal prostates: Ex vivo study with human prostates, J. Ultrasound Med. 35 (2016) 2165–2177.
[10] X. Gao, C. Tao, X. Wang, X. Liu, Quantitative imaging of microvasculature in deep tissue with a spectrum-based photo-acoustic microscopy, Opt. Lett. 40 (2015) 970–973.
[11] G. Xu, I.A. Dar, C. Tao, X. Liu, C.X. Deng, X. Wang, Photoacoustic spectrum analysis for microstructure characterization in biological tissue: a feasibility study, Appl. Phys. Lett. 101 (2012), 221102.
[12] M.N. Fadhel, E. Hysi, J. Zalev, M.C. Kolios, Photoacoustic simulations of microvascular bleeding: spectral analysis and its application for monitoring vascular-targeted treatments, J. Biomed. Opt. 24 (2019) 1–8.
[13] M.N. Fadhel, S. Appak Baskoy, Y. Wang, E. Hysi, M.C. Kolios, Use of photoacoustic imaging for monitoring vascular disrupting cancer treatments, J. Biophotonics. (2020).

[14] M.N. Fadhel, M.C. Kolios, Photoacoustic speckle and spectral analysis of vasculature trees, : IFMBE Proc. (2015) 1084–1087.
[15] N. Rathi, S. Sinha, Quantitative tissue characterization using discrete wavelet transform of photoacoustic signals: a feasibility study, Signal Image Video, Process 13 (2019) 1357–1365.
[16] M.J. Moore, E. Hysi, M.N. Fadhel, S. El-Rass, Y. Xiao, X.-Y. Wen, M.C. Kolios, Photoacoustic F-mode imaging for scale specific contrast in biological systems, Commun. Phys. 2 (2019) 1–10.
[17] M. Khairalseed, K. Hoyt, J. Ormachea, A. Terrazas, K.J. Parker, H-scan sensitivity to scattering size, J. Med. Imaging 4 (2017), 043501.
[18] L. Basavarajappa, J. Baek, S. Reddy, J. Song, H. Tai, G. Rijal, K.J. Parker, K. Hoyt, Multiparametric ultrasound imaging for the assessment of normal versus steatotic livers, Sci. Rep. 11 (2021) 2655.
[19] J. Baek, S.S. Poul, L. Basavarajappa, S. Reddy, H. Tai, K. Hoyt, K.J. Parker, Clusters of ultrasound scattering parameters for the classification of steatotic and normal livers, Ultrasound Med. Biol. 47 (2021) 3014–3027.
[20] J. Baek, L. Basavarajappa, K. Hoyt, K.J. Parker, Disease-specific imaging utilizing support vector machine classification of H-scan parameters: assessment of steatosis in a rat model, IEEE Trans. Ultrason. Ferroelectr. Freq. Control. 69 (2022) 720–731.
[21] M. Khairalseed, K. Javed, G. Jashkaran, J.-W. Kim, K.J. Parker, K. Hoyt, Monitoring early breast cancer response to neoadjuvant therapy using H-scan ultrasound imaging: preliminary preclinical results, J. Ultrasound Med. 38 (2019) 1259–1268.
[22] M. Khairalseed, F. Xiong, J.-W. Kim, R.F. Mattrey, K.J. Parker, K. Hoyt, Spatial angular compounding technique for H-scan ultrasound imaging, Ultrasound Med. Biol. 44 (2018) 267–277.
[23] H. Tai, J. Song, J. Li, S. Reddy, M. Khairalseed, K. Hoyt, Three-dimensional H-scan ultrasound imaging of early breast cancer response to neoadjuvant therapy in a murine model, Invest. Radiol. 57 (2022) 222–232.
[24] P.M. Morse, K.U. Ingard, Theoretical acoustics, McGraw-Hill, New York, 1968.
[25] G.B. Arfken, H.-J. Weber, Mathematical methods for physicists, Academic, San Diego, 1995.
[26] M. Xu, Y. Xu, L.V. Wang, Time-domain reconstruction algorithms and numerical simulations for thermoacoustic tomography in various geometries, IEEE Trans. Biomed. Eng. 50 (2003) 1086–1099.
[27] M. Xu, L.V. Wang, Universal back-projection algorithm for photoacoustic computed tomography, Phys. Rev. E Stat. Nonlin. Soft Matter Phys. 71 (2005), 016706.
[28] L. Basavarajappa, K. Hoyt, High-frequency quantitative photoacoustic imaging and pixel-level tissue classification, Proc. IEEE Int Symp. Biomed. Imaging 1 (2020) 308–311.
[29] E. Hysi, M.N. Fadhel, M.J. Moore, J. Zalev, E.M. Strohm, M.C. Kolios, Insights into photoacoustic speckle and applications in tumor characterization, Photoacoustics 14 (2019) 37–48.
[30] B.E. Treeby, Acoustic attenuation compensation in photoacoustic tomography using time-variant filtering, J. Biomed. Opt. 18 (2013), 036008.
[31] E. Hysi, R.K. Saha, M.C. Kolios, Photoacoustic ultrasound spectroscopy for assessing red blood cell aggregation and oxygenation, J. Biomed. Opt. 17 (2012), 125006.
[32] E. Hysi, R.K. Saha, M.C. Kolios, On the use of photoacoustics to detect red blood cell aggregation, Biomed. Opt. Express 3 (2012) 2326–2338.
[33] E. Hysi, L.A. Wirtzfeld, J.P. May, E. Undzys, S.-D. Li, M.C. Kolios, Photoacoustic signal characterization of cancer treatment response: correlation with changes in tumor oxygenation, Photoacoustics 5 (2017) 25–35.
[34] G. Xu, Z.-X. Meng, J.-D. Lin, C.X. Deng, P.L. Carson, J.B. Fowlkes, C. Tao, X. Liu, X. Wang, High resolution physio-chemical tissue analysis: towards non-invasive in vivo biopsy, Sci. Rep. 6 (2016) 16937.

Lokesh Basavarajappa is Research Scientist in the Department of Bioengineering at the University of Texas and Dallas. He received a BS and MS degree from Visvesvaraya Technological University, Belgaum, India, in 2012 and 2014, respectively, and a PhD degree in applied mechanics (Biomedical Engineering Group) from the Indian Institute of Technology Madras, Chennai, India, in 2018. His research interests include biomedical ultrasound, quantitative ultrasound, ultrasound elastography, ultrasound therapy, and photoacoustic imaging.

Kenneth Hoyt is an Associate Professor in the Department of Bioengineering at the University of Texas and Dallas. He received a BS degree in Electrical Engineering from Drexel University (Philadelphia, PA) in 2001, followed by a PhD degree in Biomedical Engineering in 2005 from the same institution. He did a postdoctoral fellowship in the Department of Electrical and Computer Engineering at the University of Rochester. Dr. Hoyt was faculty in the Department of Radiology at the University of Alabama at Birmingham (UAB) from 2008 to 2015. During this tenure he also received an MBA degree from the School of Business (2011). In short, Dr. Hoyt's research focuses on the development of novel ultrasound imaging strategies for improved management of human disease.